Available online at www.sciencedirect.com
SCIENCE DIRECT®
Journal of Solid State Chemistry 177 (2004) 207–215
JOURNAL OF SOLID STATE CHEMISTRY
http://elsevier.com/locate/jssc

Electrical conductivity and thermopower of Fe-phosphate compounds with the lazulite-type structure

E. Schmidbauer[a,*] and P. Schmid-Beurmann[b]

[a] Department für Geo- und Umweltwissenschaften, Sektion Geophysik, Universität München, Theresienstr.41, München 80333, Germany
[b] Institut für Geowissenschaften, Universität Kiel, Ohlshausenstr. 40, Kiel 24098, Germany

Received 14 January 2003; received in revised form 8 July 2003; accepted 10 July 2003

Abstract

Measurements of the electrical DC and AC conductivities were performed on three Fe-phosphate compounds in the temperature range $\sim 210\,K \leqslant T \leqslant \sim 450\,K$. The Fe-phosphates are semiconducting with activation energy of DC conductivity σ_{DC} of $E_A \sim 0.35-0.45\,eV$. For α-Fe_2PO_4O, the AC conductivity σ_{AC} in the low-temperature range is considerably enhanced relative to σ_{DC}. The frequency dependence of σ_{AC} can be described by an approximate power law. For the same compound, the thermopower Θ (Seebeck effect) was found to be positive in the range $\sim 330\,K \leqslant T \leqslant \sim 700\,K$, i.e. seemingly p-type conduction occurs; at $T > 700\,K$, Θ appears to become negative. The results are described in terms of a small polaron hopping model between localized states with electron transfer of the type $Fe^{2+} \rightarrow Fe^{3+}$ with Fe^{2+} as donors. In this model Θ can be described suggesting equal concentrations of Fe^{2+} and Fe^{3+} to take part in conduction.

Keywords: Electrical conductivity; Electron hopping; Thermopower; Fe-phosphates; Lazulite-type structure

1. Introduction

A variety of Fe-rich silicates with mixed-valence Fe cations are known to exhibit electron exchange between Fe^{2+} and Fe^{3+} cations as established by ^{57}Fe Mössbauer spectroscopy. Such compounds are for instance the minerals ilvaite, deerite and acmite [1]. Ilvaite shows a comparatively high electrical conductivity [2,3]. There are some other Fe-containing minerals and neighbored compounds which may also be suitable candidates for this effect. Among these are Fe-phosphates which crystallize in the lazulite-type structure.

One of these compounds is the metastable oxyphosphate β-$Fe^{2+}Fe^{3+}PO_4O$. It was found by ^{57}Fe Mössbauer spectroscopy to exhibit electron exchange $Fe^{2+} \rightarrow Fe^{3+}$ above $\sim 212°C$ [4]. For the stable modification α-$Fe^{2+}Fe^{3+}PO_4O$, no electron transfer could be detected by ^{57}Fe Mössbauer spectroscopy [5,6]. This result was explained by the fact that both cations populate non-equivalent lattice sites. Several different structures exist which are neighbored to β-Fe_2PO_4O. They arise by introduction of OH-groups into the structure. One of these compounds is the mixed-valence mineral barbosalite, $Fe^{2+}Fe^{3+}{}_2(PO_4)_2(OH)_2$. A series of solid solutions can be generated between β-Fe_2PO_4O and $Fe^{3+}{}_4(PO_4)_3(OH)_3$ with compositions $x3(Fe^{2+}Fe^{3+}(PO_4)O)$ $(1-x)Fe^{3+}{}_4(PO_4)_3(OH)_3$ (or $Fe^{3+}{}_{4-x}Fe^{2+}{}_{3x}(PO_4)_3(OH)_{3-3x}O_{3x}$), $0.18 < x < 0.60$ [7,8]. All these compounds are characterized by the presence of Fe^{2+} and Fe^{3+}. Any electron transfer between both cations, sensed by Mössbauer spectroscopy, refers probably to localized exchange between cation pairs. Whether long-range processes occur remains unclear.

Long-range electron transport of the type $Fe^{2+} \rightarrow Fe^{3+}$ affects most probably electrical conduction. For this reason, measurements of the electrical conductivity can provide information on this kind of electron exchange. The latter process may not be measurable by the Mössbauer effect if a rather low concentration of Fe is involved. On the other hand, electrical conduction can be essentially affected in this case. We analyzed electrical conductivity on three Fe-phosphate compositions with mixed valences of Fe ions, in order to test the effect on long-range electron exchange. Furthermore,

*Corresponding author. Fax: +49-89-2180-4205.
E-mail address: schmidba@alice.geophysik.uni-muenchen.de (E. Schmidbauer).

0022-4596/$ - see front matter © 2003 Published by Elsevier Inc.
doi:10.1016/j.jssc.2003.07.006

for one compound the thermopower (Seebeck effect) was determined, which supplies further independent information of charge transport.

α-$Fe^{2+}Fe^{3+}PO_4O$: This compound crystallizes in the orthorhombic structure (space group *Pnma*) with lattice constants $a = 7.378$ Å, $b = 6.445$ Å, $c = 7.471$ Å. Typical features of the structure are zig-zag chains of alternating face-linked $Fe^{2+}O_6$ and $Fe^{3+}O_6$ octahedra running parallel to the [010] direction. Fe^{2+} are situated on 4a and Fe^{3+} on 4c positions of the orthorhombic cell, i.e. both kinds of ions populate crystallographically non-equivalent sites. P ions are located in PO_4 tetrahedra corner-linked to octahedra (Fig. 1). An antiferromagnetic transition at 220 K was established by Mössbauer spectroscopy and by magnetic results [6]. From X-ray diffraction analysis an Fe separation of Fe–Fe = 2.92 Å was found across the linked face of two octahedra which is below that for Fe_3O_4 on octahedral sites of the spinel lattice (2.96 Å). Contrary to Fe_3O_4, no electron exchange of the type $Fe^{2+} \rightarrow Fe^{3+}$ was found from ^{57}Fe Mössbauer spectra as mentioned.

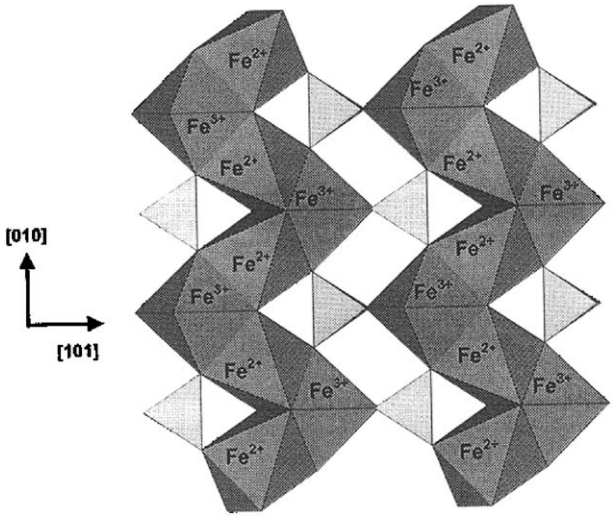

Fig. 1. Typical features of the arrangement of FeO_6 octahedra in α-Fe_2PO_4O. P cations are located in tetrahedra (after [5]).

$Fe^{2+}Fe^{3+}{}_2(PO_4)_2(OH)_2$ (barbosalite): The structure of this mineral is monoclinic. Here, characteristic straight chains of alternating face-linked $Fe^{2+}O_6$ and $Fe^{3+}O_6$ octahedra extend along [110] (Fig. 2a). However, there are oxygen octahedra with ordered cation vacancies.

$Fe^{3+}{}_{4-x}Fe^{2+}{}_{3x}(PO_4)_3(OH)_{3-3x}O_{3x}$, $x = 0.58$: One end member of the series is β-$Fe^{2+}Fe^{3+}PO_4O$ and the other one $Fe^{3+}{}_4(PO_4)_3(OH)_3$, as mentioned. For the monoclinic β-Fe_2PO_4O, Fig. 2b displays typical features of straight chains of alternating face-linked $Fe^{2+}O_6$ and $Fe^{3+}O_6$ octahedra along [001]. The metastable β-Fe_2PO_4O, which transforms above 142°C to a tetragonal structure and at ~600°C to α-Fe_2PO_4O, exhibits a separation Fe–Fe = 2.67 Å, considerably smaller than in α-Fe_2PO_4O and both Fe^{2+} and Fe^{3+} are on equivalent sites of the structure. Mössbauer spectroscopic analyses showed rapid electron transfer above 212°C because only '$Fe^{2.5+}$' could be established [6] as mentioned. The characteristics of the other end member of the related series, the monoclinic $Fe^{3+}{}_4(PO_4)_3(OH)_3$, are seen from Fig. 2d; also here straight chains occur along [001], however only $Fe^{3+}O_6$ octahedra and cation vacancies exist. The solid solution $x = 0.58$ is tetragonal; it exhibits also straight chains of face-linked $Fe^{2+}O_6$ and $Fe^{3+}O_6$ octahedra, but there are disordered cation vacancies (only ~88% of cation sites are occupied by

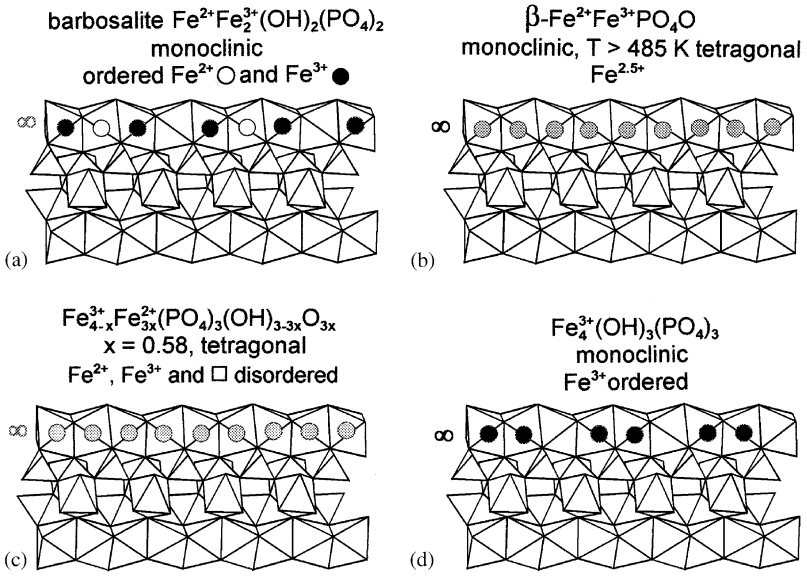

Fig. 2. Characteristic features of some Fe-phosphates which suggest one-dimensional charge transport of the type $Fe^{2+} \rightarrow Fe^{3+}$ (□ = vacancy); (a) structure after [34,35], (b) structure after [36], (c) structure after [8], (d) structure after [37,38].

Fe cations). Hence, a mixture of $Fe^{2+}O_6$, $Fe^{3+}O_6$ and cation vacancies exists along the chains; the fraction of concentration $[Fe^{2+}]/[\sum Fe] = 0.34$. The distance Fe–Fe ~ 2.65 Å [8] is below that for β-Fe_2PO_4O (Fig. 2c).

Measurements of the electrical conductivity σ showed α-Fe_2PO_4O to be a semiconductor with $\sigma(330\,K) \sim 4.5 \times 10^{-7}\,\Omega^{-1}\,cm^{-1}$ and an activation energy $E_A \sim 0.35$ eV in the temperature range $\sim$330–625 K. By contrast, the metastable tetragonal β-Fe_2PO_4O has a relatively high $\sigma(330\,K) \sim 3 \times 10^{-3}\,\Omega^{-1}\,cm^{-1}$ with $E_A = 0.20$ eV in the range 150–305 K and $E_A = 0.32$ eV from 305 to 570 K [4]. Electrical conduction is thought to be effected by electron hopping between localized levels of Fe^{2+} and Fe^{3+} cations with a transition from one-dimensional (1D) to three-dimensional (3D) conduction at 305 K.

In the following we present results of electrical conductivity measurements on the above compositions. While DC conductivity gives information on charge transfer processes taking place from electrode to electrode, AC data supply further insight into electron hopping processes in clusters of variable length, when the frequency is varied. In addition, the thermopower was measured to get additional information about the charge transport mechanism. We discuss conduction processes in more detail by describing experimental data by theoretical models, derived for electron hopping between localized levels, lying intermediate between the valence and conduction bands.

2. Sample preparation and experimentals

2.1. Sample preparation

α-Fe_2PO_4O was prepared from synthetic powders by heating at 900°C for 3d. $Fe_3(PO_4)_2(OH)_2$ (barbosalite) was prepared hydrothermally at 400°C and 3 kb. The solid solution $Fe^{3+}_{4-x}Fe^{2+}_{3x}(PO_4)_3(OH)_{3-3x}O_{3x}$, $x = 0.58$, was prepared by the same technique at 600°C and 3 kb. The resulting product contained $\sim$5% α-Fe_2O_3. Details of the preparation technique are described in Ref. [8]. The samples were pressed powders in the shape of pellets of $\sim$6 mm diameter and $\sim$1 mm thick. The effective bulk density was estimated to be $\sim$60–80% of the theoretical density.

2.2. Experimentals

Impedance spectroscopy was used to determine the DC conductivity by extrapolating AC data to zero frequency. The measurements were performed fully automatic applying a Hewlett Packard 4284A high precision LCR meter (20 Hz–1 MHz), utilizing the four-terminal pair AC impedance measurement technique at temperatures $T < 300$ K and a two-terminal method with very short leads at $T > 300$ K. Electrical contacts were made by covering opposite sides of a sample with Pt paste. A minicryostat was applied for sample temperatures below room temperature and a minifurnace for higher temperatures. In the latter case N_2 (99.999%) gas atmosphere was used for sample protection.

Thermovoltage U_{th} measurements were carried out in the temperature range $330\,K \leqslant T \leqslant 690\,K$. At room temperature the sample resistance was too high for reliable measurements. Samples were clamped between Pt-plates (diameter $\sim$6 mm) and Pt-leads were used. One Pt-plate was heated with a microheater to generate a T difference ΔT between both sample faces. The whole sample cell was inserted in a tube furnace. Temperatures were measured with two thermocouples attached to the Pt-plates. The thermocouple thermovoltages and the sample thermovoltage U_{th} were measured with HP34420A nanovoltmeters (input resistance $> 10^{10}\,\Omega$). Five ΔT values in the range 0.5–3 K were generated and the thermopower Θ ($\Theta = U_{th}/\Delta T$) was determined from the slope U_{th} vs. ΔT in order to eliminate spurious offset voltages. Absolute Θ values are given taking into account experimental results of the thermovoltage of Pt [9].

3. Results

3.1. Complex impedance plane analysis

3.1.1. α-$Fe^{2+}Fe^{3+}PO_4O$

AC data are presented in Fig. 3a in the complex-plane impedance representation. The real part of the impedance, Z', is plotted against the imaginary part, Z''; parameter is the frequency. One semicircular arc is expected if a single conduction mechanism exists [10]. Each further charge transfer mechanism supplies an additional arc. From Fig. 3a it can be seen that in fact a superposition of two semicircular arcs exists which are designated by 1 and 2. Hence, two conduction processes are simultaneously acting. The arc 1 is due to the bulk conduction mechanism while the arc 2 may be due either to grain boundary effects or to the surface layer sample electrode. This distinction can be made on the basis of the experimental capacitance C, related to each arc. The arc 1 exhibits $C \sim 1$ pF/cm while arc 2 gives $C > 50$ pF/cm. The low bulk value of C is expected, when a relative electrical permittivity $\varepsilon < 50$ is presumed, which appears to be reasonable. We could not detect any major difference in the formation of arc 2 when 1 V or 20 mV was applied at the sample.

From the data of arc 1 we determined the bulk DC resistivity, extrapolating arc 1 to zero frequency and taking the intersection point on the Z'-axis. For this purpose a fit program can be used [11], applying for the conduction processes the model of an equivalent series

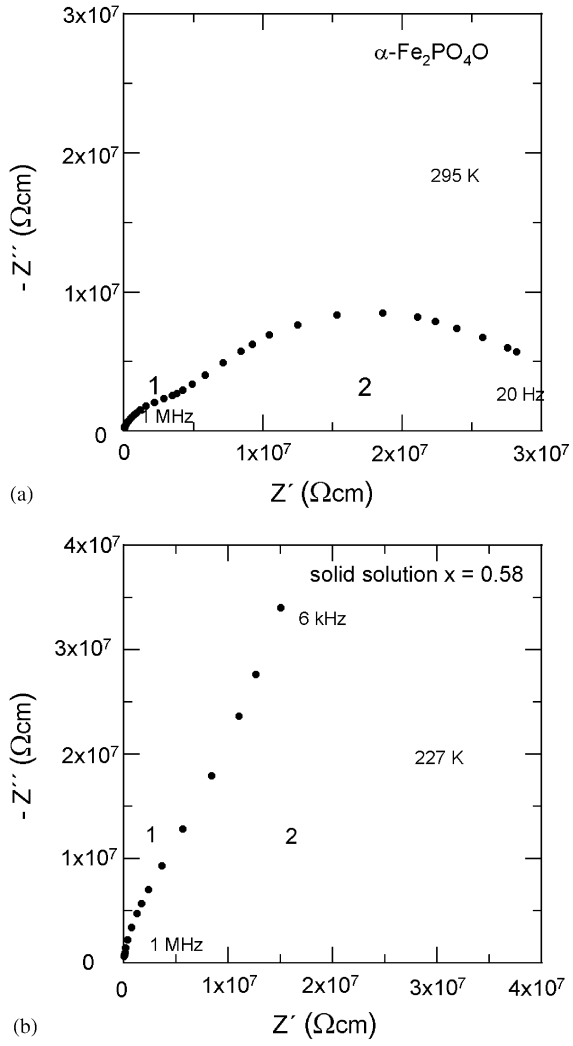

Fig. 3. Real part, Z', against the imaginary part, Z'', of the impedance on the complex impedance plane. Parameter is the frequency in the range 20 Hz–1 MHz. (a) α-Fe_2PO_5, (b) solid solution $x = 0.58$ (see text).

circuit consisting of two subcircuits, each formed in principle by a resistor in parallel to a capacitor [10].

3.1.2. $Fe^{2+}Fe^{3+}{}_2(PO_4)_2(OH)_2$ (barbosalite)

Impedance data at room temperature point to results for Z' and Z'' which are above the limit that could be measured with our LCR-meter. The DC conductivity is expected to be σ_{DC} (295 K) $< 10^{-8}\,\Omega^{-1}\,cm^{-1}$.

3.1.3. $Fe^{3+}{}_{4-x}Fe^{2+}{}_{3x}(PO_4)_3(OH)_{3-3x}O_{3x}$, $x = 0.58$

Experimental data of Z' and Z'' are presented in Fig. 3b. In contrast to α-Fe_2PO_4O, a barely visible semicircular arc 1 is seen at 227 K. For clarity, the plot is only presented down to 6 kHz. The arc 2 is by far larger than arc 1. The DC resistivity is adequately determined by linear extrapolation of arc 2 to infinite frequency, taking into account that arc 1 is directly followed by arc 2 on the complex impedance plane. Due to this difficulty, data points can only be taken with a reduced accuracy of an estimated ~15–20%. This error is, however, tolerable because the DC conductivity is varying orders of magnitude with temperature.

3.2. DC conductivity

Fig. 4a shows the logarithm of the extrapolated DC conductivity σ_{DC} vs. the reciprocal of temperature T for α-Fe_2PO_4O. The graph exhibits an activated behavior according to $\sigma_{DC} = \sigma_0 \exp(-E_A/k_B T)$ between ~265 and ~400 K with activation energy $E_A = 0.35$ eV. At $T \sim 400$ K a change in slope appears to occur with $E_A = 0.45$ eV for $T > 400$ K. These results were reproducible. Fig. 4b displays the respective data for the solid solution $x = 0.58$ which exhibits $E_A = 0.37$ eV. From the graphs it can be seen that σ_{DC} (300 K)

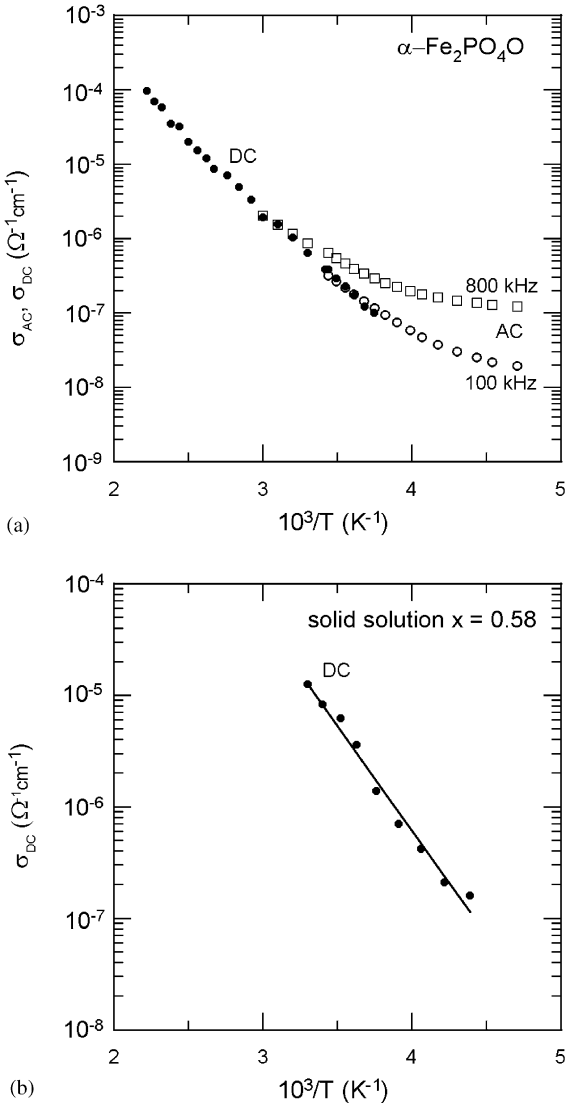

Fig. 4. (a) Logarithm of the DC conductivity σ_{DC} and of the AC conductivity $\sigma_{AC}(\omega)$ vs. the reciprocal of temperature $1/T$ for α-Fe_2PO_5 ; (b) $\log \sigma_{DC}$ vs. $1/T$ for composition $x = 0.58$.

$\sim 6\times10^{-7}\,\Omega^{-1}\,cm^{-1}$ for α-Fe_2PO_4O and σ_{DC} (300 K) $\sim 1\times10^{-5}\,\Omega^{-1}\,cm^{-1}$ for $x=0.58$, i.e. the latter compound has a clear higher DC conductivity than the former.

It is tempting to relate the conductivity predominantly to long-range electron hopping between localized levels of Fe^{2+} and Fe^{3+} along the octahedral chains (Figs. 1 and 2(a)–(d)). In this case the low conductivity of barbosalite can be understood because of ordered cation vacancies along a chain of ordered $Fe^{2+}O_6$ and $Fe^{3+}O_6$ octahedra at room temperature, which may largely suppress long-range electron transport, while possibly electron hopping takes place to a certain degree between pairs of nearest neighbor Fe^{2+} and Fe^{3+}.

A linear relation $\log\sigma_{DC}-1/T$ is compatible with a possible 1D conduction. Such a relation is predicted for conduction in infinite chains with disorder where only hopping-type charge transport is possible [12,13].

3.3. AC conductivity

We could determine the AC conductivity $\sigma_{AC}(\omega)$ ($\omega=2\pi\nu$ with ν = frequency) at higher frequencies adequately only for α-Fe_2PO_4O in the temperature interval in question, because merely in this case it could be ascertained that the data refer to the bulk semicircular arc 1 (Fig. 3). From the graph in Fig. 4a it can be recognized that $\sigma_{AC}(\omega)$ exhibits a strong frequency dependence. At low temperatures there is an enhanced $\sigma_{AC}(\omega)$ for 100 and 800 kHz relative to σ_{DC}, while $\sigma_{AC}(\omega)$ approaches the values of σ_{DC} at higher temperatures. For this comparison it is tacitly assumed that a largely linear extrapolation of σ_{DC} towards lower temperatures can be made. The temperatures where σ_{DC} and $\sigma_{AC}(\omega)$ become identical are evidently frequency dependent. Fig. 5 presents the variation of $\sigma_{AC}(\omega)$ with frequency in a log–log representation for different temperatures. At higher frequencies, an approximately linear relationship appears to hold. The slope s is between 0.35 and 0.88. Theoretical hopping models lead to a relation

$$\sigma'(\omega)\propto A\omega^{s}, \tag{1}$$

where A is a constant weakly varying with temperature, as does also the exponent s (reviews [14,15]). In general, $\sigma'(\omega)$ is given by $\sigma'(\omega)=\sigma_{AC}(\omega)-\sigma_{DC}$, where $\sigma_{AC}(\omega)$ is the measured AC conductivity. Here, σ_{DC} is thought to arise from a conduction process quite different from $\sigma_{AC}(\omega)$. If, as in our case, both are presumed to be due in principle to the same conduction mechanism, i.e. electron hopping, with $\sigma_{DC}=\lim_{\omega\to0}\sigma_{AC}(\omega)$, such a difference is not justified [16,17]. Theoretically, saturation of $\sigma_{AC}(\omega)$ is expected for $\omega\gg1$ MHz [17]. The relation of Eq. (1) is frequently found to be approximately followed by a large number of amorphous and disordered semiconductors with $s<1$. For the relation to hold it is sufficient that the involved electron hopping

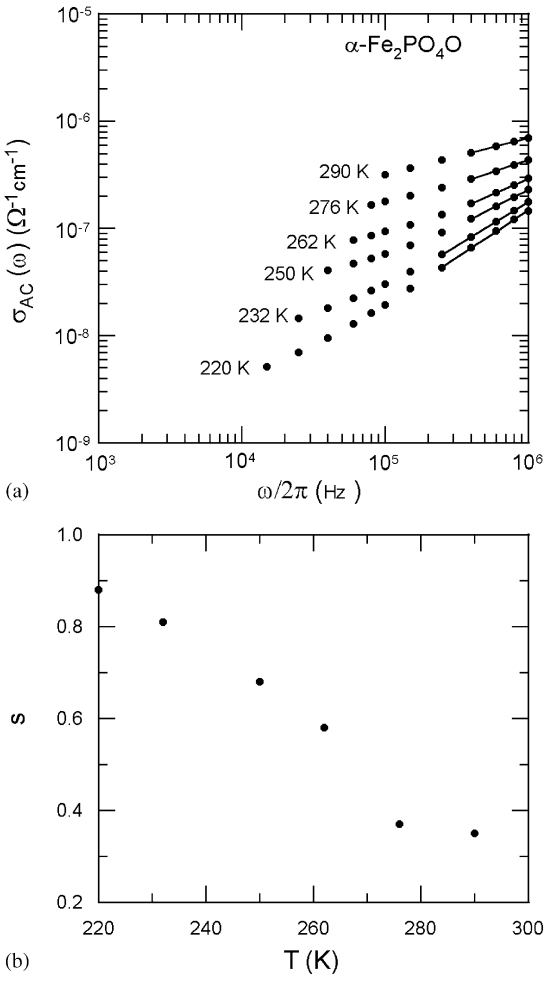

Fig. 5. (a) Variation of $\sigma_{AC}(\omega)$ with frequency on a log–log scale for various temperatures; (b) temperature dependence of the slope s marked in (a) by straight lines.

processes have a distribution of hopping relaxation times. From Fig. 5b, a clear trend towards higher values of the exponent s is seen on lowering the temperature, although experimental results are only available in a restricted temperature region. For composition $x=0.58$, we could not at 227 K detect any notable difference between σ_{DC} and $\sigma_{AC}(\omega)$ for 1 MHz, i.e. if there is dispersion it may occur at $T<227$ K.

3.4. Thermopower Θ

The thermopower Θ of α-Fe_2PO_4O could be measured only above room temperature. Below $\sim$340 K the high sample resistance did not allow reliable measurements. Experimental results are presented in the form Θ vs. $1/T$ in Fig. 6. Θ is positive at $T<700$ K with $\Theta(360\,K)\sim+90\,\mu V/K$; for temperatures above $\sim$700 K, Θ may become negative. There is a marked temperature dependence with a convex curve which we tentatively approximate by straight lines in the low and high

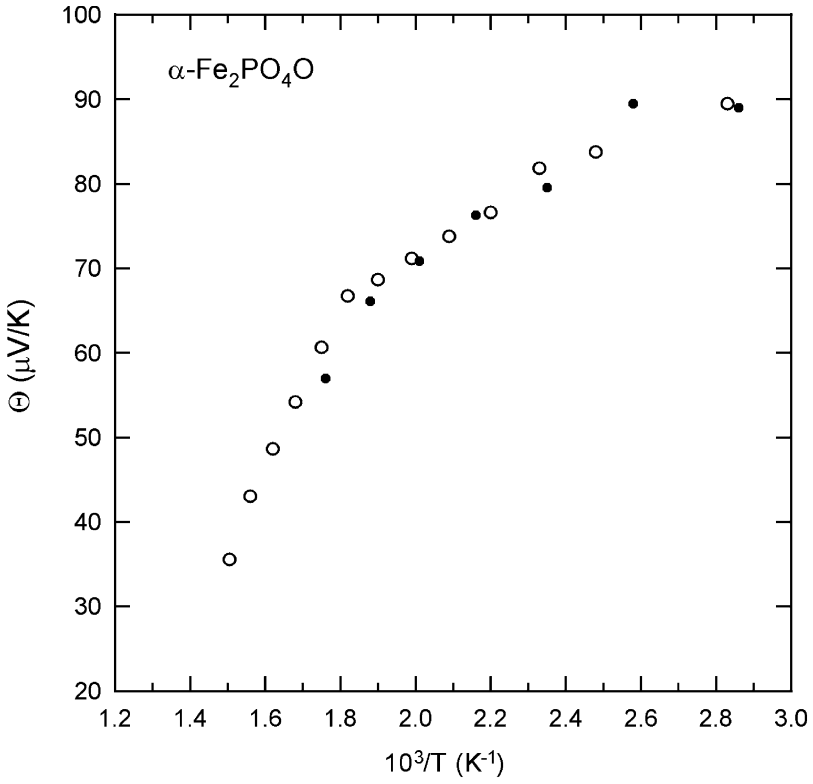

Fig. 6. Temperature dependence of the thermopower of α-Fe_2PO_5; ● first run, ○ second run.

temperature ranges. The data can be described by the relation

$$\Theta = (k_B/|e|)(E_\Theta/k_BT + A^*), \quad (2)$$

where k_B is Boltzmann's constant, e is the electronic charge, E_Θ is the thermopower activation energy and A^* is a constant. Such a law is predicted for hopping conduction of small polarons [18]. No general derivation from first principles appears to have been given yet. At higher temperatures, the hopping activation energy of the DC conductivity of small polarons is composed of two contributions $W = E_H + E_D/2$, where E_H is the hopping activation energy due to polarization and E_D is the spread of localized energy states by random fields, while in the activation energy for Θ the contribution E_H does not appear [18]. At low temperatures we extract from the straight line $E_\Theta = 0.024\,eV$ and $A^* = -0.24$ (resulting in a contribution to Θ of $\sim -21\,\mu V/K$), while at high temperatures it follows $E_\Theta = 0.13\,eV$ and $A^* = -2.44$ (giving a contribution to Θ of $\sim -210\,\mu V/K$). There is a break of the straight lines at $\sim 550\,K$. It does not coincide with that for σ_{DC} at $\sim 400\,K$. The relation of Eq. (2) was applied to interpret the temperature variation of Θ for hopping-type conduction in disordered semiconductors such as in $La_2NiO_{4+\gamma}$ [19] and in several Mn-containing perovskite-type oxides in the insulating phase above the magnetic order temperature [20–22].

It should be noted that a relation $\Theta \propto 1/T$ is also expected in the case of band conduction, if for instance a charge carrier is excited by thermal activation from a localized state in the neighborhood of the Fermi level into a conduction band. Hence, theoretically the high temperature Θ may be due to band conduction. For glasses with conduction proceeding by electron hopping between mixed-valence transition metal ions, frequently an electron transition is discussed from a band edge of localized states to a state beyond the so-called mobility edge to extend states by thermal excitation, which leads to a term $(k_B/e)(E_0/k_BT)$ in the thermopower when $E_0 \gg k_BT$ [18].

4. Discussion

4.1. Electrical conductivity

The DC conductivity of α-Fe_2PO_4O with σ_{DC} (330 K) $\sim 2.4 \times 10^{-6}\,\Omega^{-1}\,cm^{-1}$ is higher than reported earlier where σ_{DC} (330 K) $\sim 4.5 \times 10^{-7}\,\Omega^{-1}\,cm^{-1}$ was observed [2]. Below $\sim 395\,K$, our activation energy of $E_A = 0.38\,eV$ is very close to the value of $\sim 0.35\,eV$, found by these workers for measurements between ~ 330 and $650\,K$. Electrical conduction of the hopping type $Fe^{2+} \rightarrow Fe^{3+}$ may occur by 1D or 3D charge transport. The chain structure of Fig. 1 suggests a possible 1D mechanism along [010]. However, unless

coupled hopping processes take place for the whole chain, two Fe cations with the same charge are neighbored during hopping which is very unlikely for energetic reasons. In fact a quasi-1D conduction mechanism can be thought of, when electron transfer takes place between Fe^{2+}–Fe^{3+} pairs, possibly via intervening 2*p*-orbitals of oxygen anions. Furthermore, for the hopping processes under question lattice defects can play a role. In the latter situation a clear trend regarding the dimensionality of conduction cannot be decided a priori from measurements on polycrystalline materials. The low $\sigma_{DC}(295\,K) < 10^{-8}\,\Omega^{-1}\,cm^{-1}$ of barbosalite may be related to ordered Fe vacancies in the chains of $Fe^{2+}O_6$ and $Fe^{3+}O_6$ octahedra. The enhanced $E_A = 0.45\,eV$ of α-Fe_2PO_4O at $T > 395\,K$ points to a somewhat changed charge transfer process. No break in the $\log \sigma_{DC} - 1/T$ graph was reported earlier, in contrast to β-Fe_2PO_4O at $\sim 305\,K$ [2]; for the latter compound a transition from 1D to 3D conduction was suggested to occur as mentioned. We tentatively describe the high-T part of the σ_{DC}—graph in Fig. 4a in terms of a small polaron hopping model between localized states. For $T > \Theta_D/2$ (Θ_D = Debye temperature), in the non-adiabatic approximation, the relation

$$\sigma = (\sigma_0/T)\exp(-E_A/k_B T), \tag{3}$$

$$\sigma_0 = \nu_0 e^2 (1/Rk_B) c(1-c)\exp(-2\alpha R) \tag{4}$$

should hold [23], where α is the wave function decay constant (α^{-1} = localization length of the s-like wave function suggested to describe the localized state near the Fermi level of the hopping electron), R is the hopping distance to the nearest neighbor, E_A is the activation energy, k_B is Boltzmann's constant, ν_0 is the mean optical phonon frequency with $h\nu_0 = k_B\Theta_D$ (h = Planck's constant,), e is the electronic charge, and c is the fraction of hopping sites occupied by charge carriers. In order to infer parameters from experimental data using the extrapolated σ_0, one has to make an estimate of the concentration c of charge carriers. For $T > \Theta_D/2$, the activation energy E_A for polaron hopping is composed of two contributions as mentioned above: $E_A = E_H + E_D/2$. The above model has been successfully applied to mixed-valence charge hopping processes in glasses [23–26].

Suggesting all Fe ions to take part in conduction, we have in the picture of $Fe^{2+} \rightarrow Fe^{3+}$ electron hopping for the concentration of Fe^{2+} donors and, hence, of hopping electrons $c = 0.5$. From extrapolation of the graph $\log(\sigma_{DC}T) - 1/T$ in the high-T region we found, taking $\nu_0 = 1 \times 10^{13}\,s^{-1}$, $\alpha R = 0.25$. Using approximately $R = 3.0$ Å as the distance between two neighbored Fe cations along the [010] direction taking part in hopping, it follows $\alpha^{-1} \sim 2.8$ Å as localization length for a hopping electron. Such a value is predicted for small polarons for which it is expected $\alpha^{-1} \leqslant R$ [18]. This result shows that application of Eq. (3) leads to reasonable results. Extrapolation, using the smaller slope at lower temperatures in Fig. 4a, gives a value of $\alpha^{-1} \sim 1.1$ Å. It is noteworthy that these results are obtained suggesting obviously all Fe ions to take part in conduction. The same procedure was made using data for composition $x = 0.58$. From the extrapolation with the concentration of all Fe^{2+}, i.e. $c = 0.34$, we have localization length $\alpha^{-1} = 4.8$ Å, which appears reasonable. The fact that for a given temperature σ_{DC} of composition $x = 0.58$ is far above σ_{DC} of α-Fe_2PO_4O in magnitude, although the activation energies are nearly identical, is likely to be due to the much lower intersite distance Fe–Fe ~ 2.65 Å relative to 2.92 Å. In principle, such a small separation in oxides suggests itinerant electrons, associated with metallic conductivity, unless the related bands or subbands are full. Electron hopping may occur to a higher empty band; in this case no frequency dependence of the conductivity is expected. Further measurements are necessary at low temperatures to decide this question for composition $x = 0.58$.

Quite an analogous situation as in α- and β-Fe_2PO_4O and in $x = 0.58$, is encountered in the mineral ilvaite (ideal composition $CaFe^{2+}{}_2Fe^{3+}Si_2O_8(OH)$). An arrangement of consecutive Fe^{2+}–Fe^{3+} pairs occurs at equivalent sites in straight double chains of FeO_6 octahedra along [001]. Here from conductivity measurements on a natural single crystal it is reported that $\sigma_{DC}(300\,K) = 1.8 \times 10^{-3}\,\Omega^{-1}\,cm^{-1}$ along [001] [3]. It should be noted that natural ilvaites contain always a low percentage of impurities such as Mn, Mg, Al substituting in part for Fe within the questionable chains, along which charge transport is presumed to occur in the first place by electron hopping $Fe^{2+} \rightarrow Fe^{3+}$.

For the AC conductivity, the variation of the exponent s in Eq. (1) with temperature is predicted by theories of polaron hopping. A steady increase in s with falling temperature follows from the models of correlated barrier hopping and of overlapping large polarons [14,15] with restriction $s < 1$. In the former model electron transfer takes place over the barrier between two sites by thermal activation. In the latter, for neighboring sites each has a Coulomb potential associated with it; overlapping of these potentials results in lowering of the effective barrier. In this model quantum-mechanical tunneling of polarons occurs through barriers with overlap of the polaron distortion clouds of both sites. The experimentally accessible temperature range of our samples is too restricted to allow a clear discrimination between both models.

4.2. Thermopower

When charge transport by small polaron hopping occurs between mixed-valence transition metal ions in a disordered semiconductor, a formula may be used

describing approximately Θ for $k_B T > E_D$ by

$$\Theta = (k_B/|e|)[E_H/20k_B T + S_0], \quad (5)$$

where E_H is the hopping activation energy, due to polarization, as defined earlier. The constant $S_0 = S_1 + S_2$, i.e. it consists of two contributions. $S_1 = \ln(c/(1-c))$ with c the ratio of the number of charge carriers to hopping sites (the formula is subject to the constraint that a site cannot be doubly occupied and it is valid for 1D conduction). The spin degeneracy term $S_2 = \ln((2I_n+1)/(2I_{n+1}+1))$, where for a couple of mixed-valence cations M^{n+} and $M^{(n+1)+}$ I_n = spin value of the cation M^{n+} and I_{n+1} = spin value of the cation $M^{(n+1)+}$. In our case of suggested $Fe^{2+} \rightarrow Fe^{3+}$ electron hopping ($I_n = 2$ for Fe^{2+} and $I_{n+1} = \frac{5}{2}$ for Fe^{3+}), $S_2 = \ln(\frac{5}{6})$ [24,27–31] results. The term S_0 in Eq. (5) corresponds to the constant A^* in Eq. (2) and $E_\Theta \sim E_H/20$. For $1/T \rightarrow 0$, Eq. (5) with $S_0 = S_1$, ignoring S_2, is referred to as the Heikes formula. Variations of the Heikes formula were theoretically derived, depending on the kind of electron interactions [32]. For magnetic semiconductors there is an additional term in the bracket which is for T above the magnetic order temperature T_c given by $S_{mag} = -\gamma J^2/k_B^2 T^2$; J is the exchange integral between adjacent spins with $k_B T_c = 2$ J, $\gamma = \frac{5}{3}$ and 5 for 1D and 3D models, respectively [31]. When the force constants of the ions for both hopping sites are different and the activation energy is not equally divided between both sites, a term $(E_H/k_B T)(1-\varphi)/(1+\varphi)$ arises where φ is the ratio of force constants, which results in approximately $E_H/20k_B T$ [24].

For α-Fe_2PO_4O from the spin degeneracy term a constant contribution to the thermopower of $\Theta_{spin} = -15.7\,\mu V/K$ follows, while the temperature-dependent magnetic contribution (Néel temperature $T_N \sim 220$ K) gives for 300 K a value of $\Theta_{mag} \sim -36\,\mu V/K$ and at 500 K a value of $\Theta_{mag} \sim -16\,\mu V/K$, i.e. this term is of the same order of magnitude as the spin contribution. However, the term $\Theta_{mag} \propto 1/T^2$ cannot explain the convex bending down of the graph in Fig. 6 at higher temperatures. Suppose a concentration $c = 0.5$ of electron donors Fe^{2+} in α-Fe_2PO_4O, because there are equal concentrations of Fe^{2+} and Fe^{3+} along the chains, and all Fe to take part in conduction. It follows that $S_1 = 0$ and the constant spin term in Eq. (5) gives $\Theta_{spin} = -15.7\,\mu V/K$. This value matches approximately the experimental high-T value of $\sim -21\,\mu V/K$ obtained by extrapolating the data in the low-temperature region for $1/T \rightarrow 0$. We have, furthermore, to add Θ_{mag}. Taking in a first approximation an average $\Theta_{mag} \sim -25\,\mu V/K$ in the low-T region, it follows a total of $\sim -41\,\mu V/K$. This value is about twice the above experimental value. The temperature-dependent term in Eq. (5) gives with the experimental $E_H = 0.43$ eV, extracted from σ_{DC} data, at 500 K a value of $\sim +43\,\mu V/K$ and at 300 K a value of $\sim +72\,\mu V/K$, i.e. the correct trend for the variation of Θ with T is met, although there is no quantitative agreement. On the other hand, taking the measured $E_\Theta = 0.025$ eV, from Eq. (5), $E_H = 0.50$ eV. The fact that $c = 0.5$ with equal concentrations of Fe^{2+} and Fe^{3+} leads to a qualitatively reasonable result is noteworthy. By increasing the parameter $c = [Fe^{2+}]/[Fe^{3+}]$ to $c = 0.56$, which means a slight surplus of Fe^{2+} relative to Fe^{3+}, the experimental S_0 is approximately met. One has to suppose that there is strong electron interaction along the chains in view of the high concentration of charge carriers with 1D conduction. This situation may not have been considered appropriately in the derivation of Eq. (5).

Earlier, a discussion of Θ data along the above picture was carried out for Mn-containing perovskite-type compounds in the paramagnetic insulating phase above the magnetic order temperature T_c [20–22]; here, the magnetic term Θ_{mag} [32] was not taken into account. In this temperature range, charge transport is presumed to be hole conduction, effected by electron hopping $Mn^{3+} \rightarrow Mn^{4+}$ with partly a low concentration of Mn^{4+}. Dropping Θ_{mag} may be conceivable in view of the fact that the experimental Θ follows strictly a $\Theta - 1/T$ relation. Thus, an additional term $\Theta_{mag} \propto 1/T^2$ would not fit into this result; it looks as if Θ_{mag} has cancelled for some reason. However, for another compound of this kind with various impurities, a fit to Θ data could be improved by adding a $1/T^2$ term [33].

The large negative experimental S_0 in the high-T region (Fig. 6) is doubtless related to a changed charge transport mechanism. While the magnitude of S_0 may be adequately described by a proper concentration c in Eq. (5), the experimental activation energy $E_\Theta = 0.13$ eV, giving $E_H = 2.6$ eV, can hardly be interpreted in this picture. Whether this change is related to a transition from 1D to 3D conduction, as proposed for β-Fe_2PO_4O at 305 K, is not clear.

A thermopower law with $\Theta \propto 1/T$ is also valid when 3D band conduction is the dominating charge transfer mechanism as mentioned earlier. In this situation the suggested mechanism has to be correlated to the high-T part of the σ_{DC} curve in Fig. 4a. This part can, on the other hand, adequately be interpreted in terms of the high-T Mott formula for small polarons, hence, it is not clear how this can be brought in agreement with the high E_Θ. We also have to take into account that some kind of physico-chemical alteration of the sample may occur at higher temperatures in view of the long measurement time for Θ of ~ 60 h, because no equilibrium oxygen partial pressure was possibly present in the applied N_2 protection gas. This can give rise to a changed charge transport mechanism. The Heikes formula was used to discuss the positive experimental Θ for β-Fe_2PO_4O above 375 K [2].

Applying the picture of preferred charge conduction $Fe^{2+} \rightarrow Fe^{3+}$ in α-Fe_2PO_5 along zig-zag chains in the

(010) direction (Fig. 1), for ideal α-Fe_2PO_4O all sites are occupied by Fe^{2+}–Fe^{3+} couples, as already mentioned, and the picture of simultaneous hopping $Fe^{2+} \rightarrow Fe^{3+}$ has to be applied which may proceed via 2*p*-orbitals of oxygen anions as already mentioned. The possible effect of cation and/or anion vacancies on Θ may be less prominent than for the conductivity. The localized states of Fe^{2+} and Fe^{3+} are doubtless situated between the 2*p*-oxygen valence band and the empty 4s Fe band.

5. Conclusion

Electrical conduction in three different kinds of Fe-phosphate compounds was analyzed on polycrystalline samples, using electrical DC and AC conductivity data as well as thermopower results. Preferred conduction is suggested to occur by electron hopping of the kind $Fe^{2+} \rightarrow Fe^{3+}$ preferably along FeO_6 chains, extending along the [010] direction. In fact quasi-1D conduction may take place in α-Fe_2PO_4O and composition $x = 0.58$ with electron transfer possibly via 2*p*-orbitals of O^{2-} anions. In barbosalite, the presence of ordered cation vacancies appears to hinder long-range charge transport. In view of the alternating $Fe^{2+}O_6$ and $Fe^{3+}O_6$ octahedra along the chains with Fe^{2+} as donors, which is associated with a high concentration of charge carriers, no independent hopping processes are likely in this model. Strong interaction between the electrons is expected with correlated electron hopping. This picture appears to be compatible with models of DC conductivity and thermopower. Whether lattice defects play an essential part is not quite clear. In α-Fe_2PO_4O, the relatively small distance Fe–Fe ~ 2.92 Å between octahedra along [010] and in particular in composition $x = 0.58$ with Fe–Fe ~ 2.65 Å is below the distance between Fe ions on B-sites of Fe_3O_4 (~ 2.96 Å) which exhibits a comparatively high electrical conductivity in terms of $Fe^{2+} \rightarrow Fe^{3+}$ charge transport; in our phosphates, the maximum DC conductivity is only $\sigma_{DC}(300\,K) \sim 1 \times 10^{-5}\,\Omega^{-1}\,cm^{-1}$. According to theory, structural defects within the chains can give rise to severe reduction in σ_{DC} for 1D conduction. For a more detailed study of these effects, monocrystalline samples have to be available.

Acknowledgments

This study was supported by financial help of the Deutsche Forschungsgemeinschaft.

References

[1] G. Amthauer, G.R. Rossman, Phys. Chem. Miner. 11 (1984) 37–51.
[2] J.M.D. Coey, J. Allan, K. Xuemin, N. Van Dang, S. Ghose, J. Appl. Phys. 55 (1984) 1963–1965.
[3] E. Schmidbauer, G. Amthauer, Phys. Chem. Miner. 25 (1998) 522–533.
[4] B. Ech-Chahed, F. Jeannot, B. Malaman, Ch. Gleitzer, J. Solid State Chem. 74 (1988) 47–59.
[5] R. Iraldi, G. Le Caër, D. Gleitzer, Solid State Commun. 40 (1981) 145–147.
[6] A. Modaressi, A. Courtopis, R. Gerardin, B. Malaman, Ch. Gleitzer, J. Solid State Chem. 40 (1981) 301–311.
[7] J.M.M. Millet, Catal. Rev. Sci. Eng. 40 (1998) 1–38.
[8] P. Schmid-Beurmann, J. Solid State Chem. 153 (2000) 237–247.
[9] J.P. Moore, R.S. Graves, J. Appl. Phys. 44 (1973) 1174–1178.
[10] J.R. Macdonald, Impedance Spectroscopy, Wiley, New York, 1987.
[11] Y.T. Tsai, D.H. Whitmore, Solid State Ionics 7 (1982) 129–139.
[12] J. Kurkijärvi, Phys. Rev. B 8 (1973) 922–924.
[13] W. Brenig, G.H. Dohler, H. Heyszenau, Philos. Mag. 27 (1973) 1093–1103.
[14] A.R. Long, Adv. Phys. 31 (1982) 553–637.
[15] S.R. Elliott, Adv. Phys. 36 (1987) 135–218.
[16] D. Emin, K.L. Ngai, J. Phys. Coll. C3 44 (1983) 471–475.
[17] J.C. Dyre, J. Appl. Phys. 64 (1988) 2456–2468.
[18] N.F. Mott, E.A. Davis, Electronic Processes in Non-crystalline Materials, Clarendon Press, Oxford, 1979.
[19] A. Demourges, P. Dordor, J.-P. Doumerc, J.-C. Grenier, E. Marquestaut, M. Pouchard, A. Villesuzanne, A. Wattiaux, J. Solid State Chem. 124 (1996) 199–204.
[20] M. Jaime, M.B. Salamon, M. Rubinstein, R.E. Treece, J.S. Horwitz, D.B. Chrisey, Phys. Rev. B 54 (1996) 11914–11917.
[21] M.F. Hundley, J.J. Neumeier, Phys. Rev. B 55 (1997) 11511–11515.
[22] D. Niebieskikwiat, R.D. Sanchez, J. Magn. Magn. Mater. 221 (2000) 285–292.
[23] N.F. Mott, J. Non-Cryst. Solids 1 (1968) 1–17.
[24] I.G. Austin, N.F. Mott, Adv. Phys. 18 (1969) 41–102.
[25] A. Gosh, Phys. Rev. B 41 (1990) 1479–1488.
[26] A. Gosh, Phys. Rev. B 47 (1993) 15537–15542.
[27] R.R. Heikes, A.A. Maradudin, R.C. Miller, Ann. Phys. 8 (1963) 733–746.
[28] H.-I. Yoo, H.L. Tuller, J. Phys. Chem. Solids 49 (1988) 761–766.
[29] A.J. Bosman, H.J. van Daal, Adv. Phys. 18 (1971) 41–102.
[30] J.-P. Doumerc, J. Solid State Chem. 109 (1994) 419–420.
[31] N.-L. Liu, D. Emin, Phys. Rev. 30 (1984) 3250–3256.
[32] P.M. Chaikin, G. Beni, Phys. Rev. B 13 (1976) 647–651.
[33] O.A. Yassin, S.N. Bhatia, J. Alloys Compd. 326 (2001) 69–73.
[34] G.J. Redhammer, G. Tippelt, G. Roth, W. Lottermoser, G. Amthauer, Phys. Chem. Miner. 27 (2000) 419–429.
[35] M.L. Lindberg, C.L. Christ, Acta Crystallogr. 12 (1959) 695–697.
[36] E. Elkaim, J.F. Berar, C. Gleitzer, B. Malaman, M. Ijjaali, C. Lecomte, Acta Crystallogr. B 52 (1996) 428–431.
[37] C.C. Torardi, W.M. Reiff, L. Takaks, J. Solid State Chem. 82 (1989) 203–215.
[38] M. Ijjaali, B. Malaman, C. Gleitzer, M. Pichavant, Eur. J. Solid State Inorg. Chem. 26 (1989) 73–89.